Materials Research Proceedings **8** (2018) 70-79 doi: http://dx.doi.org/10.21741/9781945291999-8

Mössbauer spectroscopic analysis of $(Nd,Pr,Dy)_2(Fe,Co,Ga)_{14}B/\alpha$-Fe permanent magnetic nanocomposites

Božidar CEKIĆ[1,a], Valentin IVANOVSKI[1,b], Mirela Maria CODESCU[2,c*], Ana UMIĆEVIĆ[1,d], Katarina ĆIRIĆ[1,e], Eugen MANTA[2,f]

[1]Institute of Nuclear Sciences Vinča, University of Belgrade, Belgrade, Serbia

[2]Research and Development National Institute for Electrical Engineering ICPE-CA 313 Splaiul Unirii, Bucharest - 3, Romania

[a]cekic@vinca.rs; [b]valiva@vinca.rs; [c]mirela.codescu@icpe-ca.ro; [d]umicev@vinca.rs; [e]kciric@vinca.rs; [f]eugen.manta@icpe-ca.ro

Keywords: NdFeB nanocomposites, XRD analysis, Mössbauer spectroscopy, Internal magnetic field, Quadrupole splitting

Abstract. In this paper, it is reported the structural and magnetic properties of $Nd_{13.7}Pr_{0.7}Dy_{0.2}Fe_{73.1}Co_{6.3}Ga_{0.4}B_{5.6}$ and $Nd_{7.7}Pr_{0.7}Dy_{0.2}Fe_{79.1}Co_{6.3}Ga_{0.4}B_{5.6}$ magnetic nanocomposites, synthesized by melt-spinning and annealing methods. The Nd-Fe-B ribbons are melt-spun at v=30 m/s in high vacuum and annealed at 715^{o}C for 4 min. in argon. Furthermore, X-ray diffraction and transmission ^{57}Fe Mössbauer spectra at RT are used to investigate the effects of substituent elements: Dy, Pr, Co, Ga on the hard magnetic properties and microstructure of both nanocomposites. Analysis of Mössbauer spectra for $Nd_{13.7}Pr_{0.7}Dy_{0.2}Fe_{73.1}Co_{6.3}Ga_{0.4}B_{5.6}$ is done in terms of ten Zeeman sextets, one paramagnetic doublet related to $Nd_{1.1}Fe_4B_4$ phase and two hyperfine magnetic fields distributions extracted from spectrum. Similar result of analysis of the second nanocomposite is obtained with eleven sextets, one doublet and one distribution. One sextet corresponds to α-Fe phase, while we have identified six iron sextets corresponding to the six distinct iron sites in the $Nd_2Fe_{14}B$ structure: $16k_1$, $16k_2$, $8j_1$, $8j_2$, 4c and 4e. The three remaining sextets belong to Fe_3B structure with three inequivalent Fe sites: Fe_I(8g), Fe_{II}(8g) and Fe_{III}(8g). The eleventh sextet of $Nd_{7.7}Pr_{0.7}Dy_{0.2}Fe_{79.1}Co_{6.3}Ga_{0.4}B_{5.6}$ belongs to FeB. All relevant parameters for both nanocomposites: magnetic hyperfine field, isomer shift and quadrupole splitting are determined for each of these sites. To highlight the thermally induced structural transformations, the quenched samples have been analysed by differential scanning calorimetry and thermo-magnetic measurements. The magnetic properties, measured at RT on the quenched and annealed ribbons, revealed the relationship between the alloy chemical composition and processing.

1. Introduction

Hard magnetic materials were divided into the group of conventional metallic and oxide magnets and the group of modern magnets based on intermetallic compounds of rare earth elements with Co and/or Fe. The importance of advanced permanent magnetic materials in many electro-, magneto-chemical and electronic applications is depending on the significant improvement of the magnetic energy density and a high coercivity or "magnetic hardness" of the new hard magnetic materials. The basis for these high-performance magnets are rare earth intermetallic phases $SmCo_5$ [1] and $Nd_2Fe_{14}B$ [2-4]. Discovered in '80, the NdFeB magnets imposed due to their remarkable magnetic performance at room temperature, but they present some disadvantages, related to their

thermal and corrosion stability [5-7], disadvantages that limit their operating regime in various applications field.

High performance $Nd_2Fe_{14}B$-based permanent magnets are produced with different composition and processing techniques, the magnetic properties of rare earths based permanent magnets being strongly dependent on their chemical composition. In this respect, any alloy contamination, especially with oxygen, occurred during processing, depletes the alloy of the rare earth elements. The first, negative consequence is the shift of the composition on the side of the phase diagram, rich in transition metals, that means a disadvantageous phase distribution. Depending on the alloy composition, the nanocomposite structures can be $Nd_2Fe_{14}B/Fe_3B$ or $Nd_2Fe_{14}B$/α-Fe or mixture of both. Many efforts are continuously devoted to improve the performance of $Nd_2Fe_{14}B$/α-Fe nanocomposite magnets. One of the most effective methods was through the compositional modification of $Nd_2Fe_{14}B$/α-Fe system [8-10]. Two main types of elements can be added to $Nd_2Fe_{14}B$/αFe composites: (a) substitutional elements such as Pr, Dy, Co, Ga and La [11,12] and (b) two different types of dopants such as Al, Cu, Zn, Ge, Sn and Ti, Zr, V, Mo, Nb and W [13-15]. Two different types of dopants, influencing microstructure in different ways, can be distinguished independently of the processing route; sintering, melt-spinning, mechanical alloying and hot worked magnets: for example, dopants M1 type as Al, Cu, Ga form binary M1-Nd or ternary M1-Fe-Nd phases and dopants M2 type as Ti, Zr, V, Mo, Nb, W form binary M2-Nd or ternary M2-Fe-B phases. Substituent and dopant elements influence the microstructure, coercivity and corrosion resistance of advanced (Nd,Pr,Dy)-(Fe,Co,Ga)-B magnets. Generally, two types of substituent elements, which replace the rare earth element or transition element sites in the hard-magnetic phase, and two types of dopant elements are distinguished for the highest value of energy density product, obtained so far [16]. Selected elements substitute the Nd-atoms (Pr and Dy) and the Fe-atoms (Co and Ga), in the hard magnetic Φ-phase. Their introduction changes the intrinsic properties; the spontaneous polarization, the Curie temperature and the magnetocrystalline anisotropy according to their solubility range within the $Nd_2Fe_{14}B$ phase.

2. Experimental

2.1 Preparation and XRD

In the Nd-Fe-B system, our studied multicomponent alloys: $Nd_{13.7}Pr_{0.7}Dy_{0.2}Fe_{73.1}Co_{6.3}Ga_{0.4}B_{5.6}$ and $Nd_{7.7}Pr_{0.7}Dy_{0.2}Fe_{79.1}Co_{6.3}Ga_{0.4}B_{5.6}$ are all based on the stoichiometric composition of $Nd_2Fe_{14}B$ hard magnetic phase. The alloys are melted using the induction furnace, Leybold - Heraeus type, in an Al_2O_3 crucible, starting from elements or masteralloys (B20-Fe, Nd84-Fe, Dy80-Fe, in wt. %). In order to avoid the oxidation of the rare earths alloys, their processing is performed in vacuum (10^{-3} – 10^{-4} mbar) and then inert atmosphere (argon, 99.95% purity), and the iron was previously deoxidized, through annealing in reducing atmosphere (hydrogen), at 800 – 850^{o}C, for 3 hours. The purity of all elements was higher than 99.8%. The ingots are remelted in high vacuum ($5\cdot10^{-4}$ – 10^{-5} mbar), by the melt-spinning technique, using a quartz crucible with the diameter nozzle of Φ = 0.4 mm and the rare earths-based ribbons are prepared under argon atmosphere (900 mbar). The technological parameters of melt-spinning process were: wheel speed v = 30 m/s, and for melt alloy ejection, an argon overpressure Δp = 0.5 bar. The obtained Nd-Fe-B based ribbon, 15-50 μm thick, 5-8 mm long and 1.5-2 mm wide, have been annealed in vacuum ($2\cdot10^{-4}$ mbar)/argon at 715^{o}C for 4 min. to improve the microstructure and the magnetic properties.

The X-ray diffraction measurements were performed on Philips PW 1050 powder diffractometer with Ni filtered Cu Kα radiation (λ = 1.5418 Å) and scintillation detector within 10−120° 2θ range in steps of 0.02°, and scanning time of 12 s per step.

Mössbauer absorption spectra were obtained in a standard transmission geometry using a source of ^{57}Co in Rh (920 MBq) at room temperature (RT). A calibration was done with laser and isomer shifts values are referred to α-Fe. The measurements were made on the powder sample contained in a Plexiglas holder; the absorbers surface densities the were 39.9 mg/cm^2 for $Nd_{13.7}Pr_{0.7}Dy_{0.2}Fe_{73.1}Co_{6.3}Ga_{0.4}B_{5.6}$ and 31.6 mg/cm^2 for $Nd_{7.7}Pr_{0.7}Dy_{0.2}Fe_{79.1}Co_{6.3}Ga_{0.4}B_{5.6}$. The data were stored in 1024 multichannel analyzer. Laser spectrums were recorded and fitted in order to recalculate channels in mm/s. Sample thickness corrections were carried out by transmission integral. The spectra have been examined by fitting data with WinNormos-Dist software that enables distribution of hyperfine parameters by histogram method and allows for Lorentz sextets and doublets on well-defined ion sites [17].

To highlight the thermally induced structural transformations, the melt-spun samples from the prepared alloys have been analysed with a DSC 204 F1 Phoenix instrument from Netzsch, Germany, at 10 K/min heating rate in the temperature range (25 - 590)^{o}C. The studied samples were placed in open crucible and heated in Ar (gas purity higher than 99.996%). Also have been performed thermo-magnetic measurements on the same samples, through vibrating sample magnetometry (VSM). The measurements were performed with a VSM 7300 Lake Shore in the temperature range (25-830)^{o}C and 800 kA/m magnetic field.

3. Results and Data Analysis

The XRD patterns of the $Nd_{13.7}Pr_{0.7}Dy_{0.2}Fe_{73.1}Co_{6.3}Ga_{0.4}B_{5.6}$ and $Nd_{7.7}Pr_{0.7}Dy_{0.2}Fe_{79.1}Co_{6.3}Ga_{0.4}B_{5.6}$ nanocomposites contain four phases and are presented on the Fig. 1. All the melt-spun alloys have amorphous structure. XRD phase analysis of both nanocomposites confirmed the presence of main hard magnetic phase $Nd_2Fe_{14}B$ (space group $P4_2/mnm$), soft magnetic phases Fe_3B and partially Fe as well as minor quantities of hard magnetic $Nd_{1.1}Fe_4B_4$ boride phase.

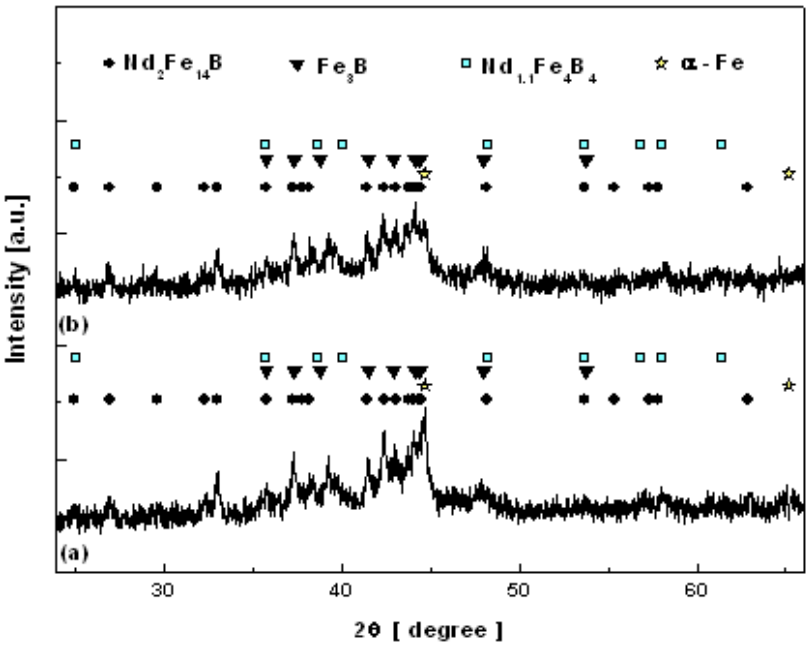

Fig. 1. XRD results of melt-spun $Nd_{13.7}Pr_{0.7}Dy_{0.2}Fe_{73.1}Co_{6.3}Ga_{0.4}B_{5.6}$ a) and $Nd_{7.7}Pr_{0.7}Dy_{0.2}Fe_{79.1}Co_{6.3}Ga_{0.4}B_{5.6}$ b) alloys after annealing treatments.

Materials Research Proceedings **8** (2018) 70-79 doi: http://dx.doi.org/10.21741/9781945291999-8

The Mössbauer absorption spectra at 294 K of both alloys are presented in Fig. 2a and Fig.2b. The spectra consist of ten Zeeman sextets and one paramagnetic doublet related to the $Nd_{1.1}Fe_4B_4$ phase. One sextet corresponds to the α-Fe phase, whereas others are attributed to six non-equivalent Fe sites in the $Nd_2Fe_{14}B$ structure, namely $16k_1$, $16k_2$, $8j_1$, $8j_2$, 4c, and 4e. The constraints associated with the computer fit of the spectra were that six subspectra were assumed in intensity ratios 4:4:2:2:1:1 The three remaining sextets belong to the Fe_3B structure with three inequivalent Fe sites $Fe_I(8g)$, $Fe_{II}(8g)$ and $Fe_{III}(8g)$. The relative intensity from crystalline phase in Fe_3B was assumed to have 1:1.4:1.5. The Mössbauer absorption spectrum at 294K of $Nd_{7.7}Pr_{0.7}Dy_{0.2}Fe_{79.1}Co_{6.3}Ga_{0.4}B_{5.6}$ (Fig. 2b), contains still one, the eleventh sextet which belongs to the FeB.

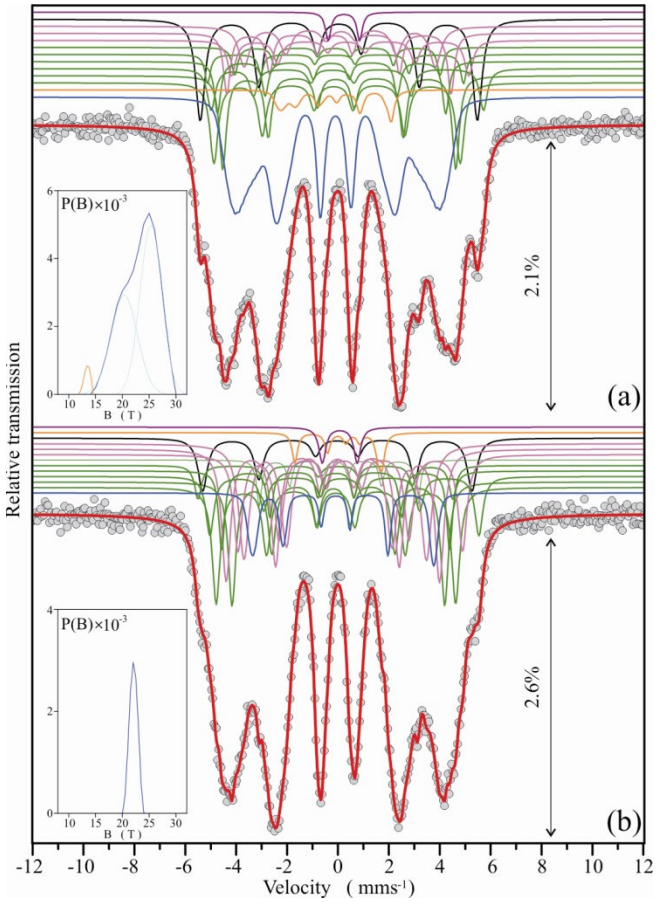

Fig. 2. Mössbauer absorption spectra at 295K in a) $Nd_{13.7}Pr_{0.7}Dy_{0.2}Fe_{73.1}Co_{6.3}Ga_{0.4}B_{5.6}$ and b) $Nd_{7.7}Pr_{0.7}Dy_{0.2}Fe_{79.1}Co_{6.3}Ga_{0.4}B_{5.6}$. Insets represent the hyperfine magnetic fields distributions at both nanocomposites.

The inset in Fig. 2 a represents two hyperfine magnetic field distributions extracted from this spectrum. It can be seen that the first distribution of FeB exhibits one peak with the highest probability of 13.4 T. The average magnetic field for this distribution is 12.64(1.91) T. The next distribution of Fe_2B exhibits two peaks with hyperfine fields of 20.4 T and 25.3 T. The average magnetic field is 23.22 (3.19) T. When the $Nd_{7.7}Pr_{0.7}Dy_{0.2}Fe_{79.1}Co_{6.3}Ga_{0.4}B_{5.6}$ nanocomposite is analyzed, the distribution exhibits one peak, corresponding to hyperfine field of 22.0 T the highest probability. The average hyperfine magnetic field calculated with this distribution is 22.07(0.72

)T. The results of the least squares fit of both nanocomposites are summarized in Table 1; the values of isomer shift (δ), quadrupole splitting ($\Delta = eQV_{ZZ}/2$), hyperfine internal magnetic field (B_{hf}) and area of each component, are reported. The results of quantitative phase XRD analysis of the nanocomposites $Nd_{13.7}Pr_{0.7}Dy_{0.2}Fe_{73.1}Co_{6.3}Ga_{0.4}B_{5.6}$ and $Nd_{7.7}Pr_{0.7}Dy_{0.2}Fe_{79.1}Co_{6.3}Ga_{0.4}B_{5.6}$ in the optimized magnetic state (Fig. 1, Table 1) suggest that the alloys are characterized by the dominant fractional amount of hard magnetic $Nd_2Fe_{14}B$ phase (60.2 % and 63.0 %). The presence of other soft and paramagnetic phases such as α-Fe, Fe_3B and $Nd_{1.1}Fe_4B_4$ were determined as well.

In addition, according to the ternary Nd-Fe-B phase diagram, this magnet contains a certain amount of $Nd_{1.1}Fe_4B_4$ and an Nd-rich phase which is essential for further hot processing.

Table 1. Selected fit of Mössbauer parameters for $Nd_{13.7}Pr_{0.7}Dy_{0.2}Fe_{73.1}Co_{6.3}Ga_{0.4}B_{5.6}$ and $Nd_{7.7}Pr_{0.7}Dy_{0.2}Fe_{79.1}Co_{6.3}Ga_{0.4}B_{5.6}$ nanocomposites.

Sample	Phase	Site	Site area [%]	Phase area [%]	I.S. [mm/s]	Magnitude of splitting Δ [mm/s]	B_{hf} [T]	Γ [mm/s]
$Nd_{13.7}Pr_{0.7}Dy_{0.2}Fe_{73.1}Co_{6.3}Ga_{0.4}B_{5.6}$	$(Nd,Pr,Dy)_2(Fe,Co,Ga)_{14}B$	16k2	9.1(8)		−0.10(1)	0.14(2)	30.0(1)	0.38(5)
		16k1	9.1(8)		−0.02(1)	0.14(2)	28.4(2)	0.33(2)
		8j2	4.6(4)		0.07(3)	0.59(4)	33.2(3)	0.37(3)
		8j1	4.6(4)		−0.26(2)	0.01(2)	27.8(1)	0.29(6)
		4c	2.3(2)		−0.11(3)	0.03(5)	31.2(2)	0.26(5)
		4e	2.3(2)	32.0	−0.09(4)	0.14(5)	25.0(2)	0.28(4)
	$(Fe,Co,Ga)_3B$	8g1	4.1(7)		0.41(5)	0.15(7)	28.9(3)	0.39(6)
		8g2	5.8(9)		−0.05(2)	0.17(6)	27.3(3)	0.32(9)
		8g3	6.2(9)	16.1	0.10(2)	−0.06(4)	23.3(1)	0.52(7)
	Fe – α	2a	13.1(9)	13.1	0.039(7)	−0.01(2)	33.77(3)	0.43(2)
			1.1(2)	1.1	0.23(2)	1.24(5)		0.26(3)
				Distributions:				
					$< B_{hf} >$	SD [T]	< I.S. >	
	$(Fe,Co,Ga)_2B$	8h	34.6	34.6	23.22	3.19	−0.06(3)	
	(Fe,Co,Ga)B	4c	3.1	3.1	12.64	1.91	−0.14(9)	
$Nd_{7.7}Pr_{0.7}Dy_{0.2}Fe_{79.1}Co_{6.3}Ga_{0.4}B_{5.6}$	$(Nd,Pr,Dy)_2(Fe,Co,Ga)_{14}B$	16k2	11.2(7)		−0.08(1)	0.00(1)	29.18(7)	0.38(2)
		16k1	11.2(7)		−0.080(6)	0.19(2)	25.91(7)	0.36(2)
		8j2	5.6(4)		0.20(1)	0.10(3)	32.78(8)	0.37(3)
		8j1	5.6(4)		−0.086(9)	−0.01(1)	27.77(8)	0.27(2)
		4c	2.8(2)		−0.24(2)	−0.51(4)	31.1(1)	0.33(4)
		4e	2.8(2)	39.2	−0.04(1)	0.11(3)	19.31(8)	0.24(2)
	$(Fe,Co,Ga)_3B$	8g1	12(1)		0.361(9)	0.25(2)	27.36(8)	0.41(3)
		8g2	16(2)		−0.111(7)	−0.18(1)	26.00(8)	0.42(3)
		8g3	17(2)	45.0	−0.028(6)	−0.16(2)	22.23(8)	0.50(2)
	Fe – α	2a	6.5(1)	6.5	−0.03(2)	0.02(3)	32.8(1)	0.44(6)
	(Fe,Co,Ga)B	4c	2.0(3)	2.0	0.30(1)	−0.56(3)	10.6(1)	0.25(4)
			1.5(2)	1.5	0.07(2)	1.37(4)		0.32(6)
				Distribution:				
					$< B_{hf} >$	SD [T]	< I.S. >	
	$(Fe,Co,Ga)_2B$	8h	5.8	5.8	22.07	0.72	0.06(3)	

The appearance of non-ferromagnetic boron rich $Nd_{1.1}Fe_4B_4$ phase, can be explained as a consequence of high boron content in the investigated alloys (above 4.2 at. %) [14]. It was found that $Nd_{1.1}Fe_4B_4$ phase forms in non-uniformly distributed heavily faulted grains of approximately the same dimensions as grains of $Nd_2Fe_{14}B$ phase [15]. It has been observed that, during recrystallization of the amorphous studied alloys after annealing at different temperatures, appears the phenomena of separation and decomposition of the B-rich phase, $Nd_{1.1}Fe_4B_4$, and the addition of Co enhanced these phenomena, increasing the content of the B-rich phase. Further, the B-rich phase dilutes the inter-grain exchange interaction resulting in a decrease of the coercivity for magnets. The $Nd_{1.1}Fe_4B_4$ phase has a very low Curie temperature (T_C = 13 K) and the magnetic properties of the magnets are drastically damaged [16]. For example, the presence of this B-rich phase in the composition of NdFeB magnetic nanocomposites has as result the decreasing of coercivity, through the dilution exchange interaction between the grains. The obtained results are in accordance with data reported by the literature [18]. The relative contents of the paramagnetic phase in both nanocomposites are 1.6% and 0.9 % (Table 1).

According to both MS and XRD results, the appearance of soft magnetic phase α-Fe of 8.5% in $Nd_{13.7}Pr_{0.7}Dy_{0.2}Fe_{73.1}Co_{6.3}Ga_{0.4}B_{5.6}$ and 5.8% in $Nd_{7.7}Pr_{0.7}Dy_{0.2}Fe_{79.1}Co_{6.3}Ga_{0.4}B_{5.6}$ is accompanied predominantly of the body centered tetragonal Fe_3B structure. These ribbons consist of a remarkable fractional amount of Fe_3B, 29.7 % and 30.3 % respectively.

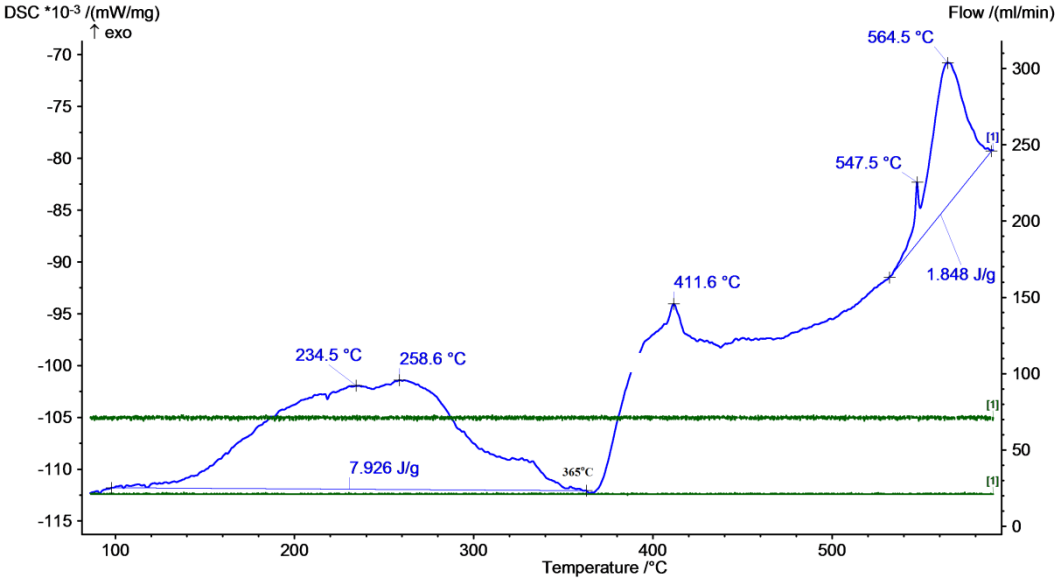

Fig. 3. The DSC curve of the $Nd_{13.7}Pr_{0.7}Dy_{0.2}Fe_{73.1}Co_{6.3}Ga_{0.4}B_{5.6}$ sample.

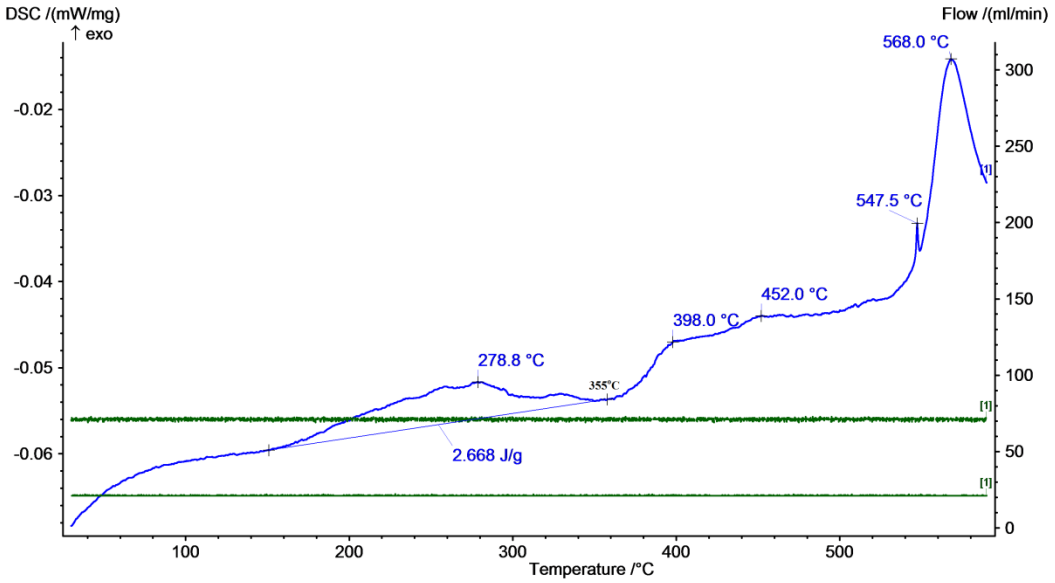

Fig. 4. The DSC curve of the $Nd_{7.7}Pr_{0.7}Dy_{0.2}Fe_{79.1}Co_{6.3}Ga_{0.4}B_{5.6}$ sample.

Samples from the ribbons prepared by melt-spinning have been investigated through DSC to monitor the thermal induced structural changes, the plotted curves being illustrated in Fig. 3 and 4. The experimental data obtained from DSC curves are in accordance with those extracted from the thermomagnetic measurements (see Fig. 5 and 6). The temperature increasing has as main effect in samples the ordering of atoms in the crystalline structure on intermetallic compounds, the process being marked by ascending curve, both in DSC investigation and in thermomagnetic measurements. The Curie point of the hard magnetic $Nd_2Fe_{14}B$ phase is represented on DSC curve trough minimum and on the thermomagnetic variations through sharp decreasing of the magnetisation.

The substitution of Fe by Co in the hard-magnetic phase is highlighted by the values of the Curie temperatures determined for the $Nd_{13.7}Pr_{0.7}Dy_{0.2}Fe_{73.1}Co_{6.3}Ga_{0.4}B_{5.6}$ and $Nd_{7.7}Pr_{0.7}Dy_{0.2}Fe_{79.1}Co_{6.3}Ga_{0.4}B_5$ samples: 365°C respectively 355°C, greater than 312°C, the Curie temperature of the $Nd_2Fe_{14}B$ compound. The crystallisation temperatures of soft magnetic phases existing in the nanocomposites are situated at 564.5°C, respectively 568°C (Fig. 3 and 4). To assure the recrystallisation also for hard magnetic phases (which take place at temperatures greater than 590°C), the annealing process was conducted at 715°C.

In order to highlight the occurrence of the exchange interaction between the soft and the hard magnetic phases from the (Nd,Pr,Dy)-(Fe,Co,Ga)-B studied nanocomposites, was determined the value of the remanent and saturation magnetisation ratio M_r/M_S, whose values, extracted from the plotted hysteresis curves, are presented in Table 2.

It can be seen that in the annealed state the soft and the magnetic phases are exchange coupled, the value of the M_r/M_S ratio being greater than 0.5.

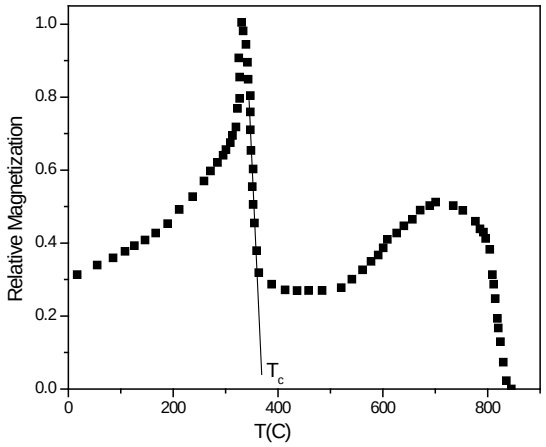

Fig. 5. Relative magnetization *vs* temperature for $Nd_{13.7}Pr_{0.7}Dy_{0.2}Fe_{73.1}Co_{6.3}Ga_{0.4}B_{5.6}$ sample.

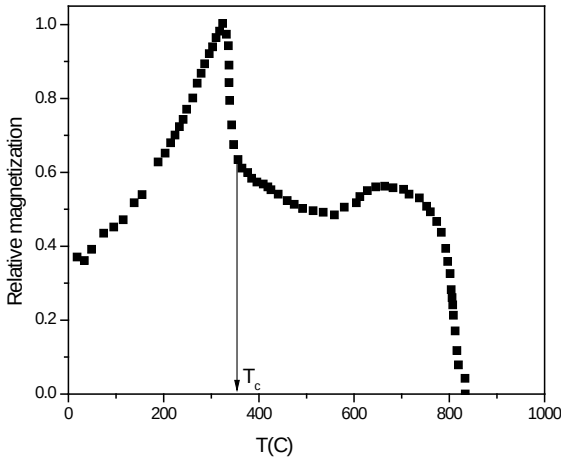

Fig. 6. Relative magnetization *vs* temperature for $Nd_{7.7}Pr_{0.7}Dy_{0.2}Fe_{79.1}Co_{6.3}Ga_{0.4}B_{5.6}$ sample.

Table 2. The main magnetic characteristics of (Nd,Pr,Dy)-(Fe,Co,Ga)-B samples.

Sample	M_s [emu/g]	M_r, [emu/g]	H_c [kA/m]	M_r/M_S ratio
$Nd_{13.7}Pr_{0.7}Dy_{0.2}Fe_{73.1}Co_{6.3}Ga_{0.4}B_{5.6}$ – melt spun	55.55	104.23	207	0.52
$Nd_{13.7}Pr_{0.7}Dy_{0.2}Fe_{73.1}Co_{6.3}Ga_{0.4}B_{5.6}$ - annealed	45.43	76.35	557	0.59
$Nd_{7.7}Pr_{0.7}Dy_{0.2}Fe_{79.1}Co_{6.3}Ga_{0.4}B_{5.6}$ – melt spun	82.36	187.25	175	0.44
$Nd_{7.7}Pr_{0.7}Dy_{0.2}Fe_{79.1}Co_{6.3}Ga_{0.4}B_{5.6}$ – annealed	85.23	136.56	233	0.62

In the case of $Nd_{13.7}Pr_{0.7}Dy_{0.2}Fe_{73.1}Co_{6.3}Ga_{0.4}B_{5.6}$ nanocomposites, the coercitive field is developed after the annealing treatment at 715^{o}C for 4 min., increasing from 207 kA/m to 557 kA/m, but this coercivity increasing is accompanied by a remanent magnetization decreasing, from 55.55 emu/g to 45.43 emu/g. In the case of $Nd_{7.7}Pr_{0.7}Dy_{0.2}Fe_{79.1}Co_{6.3}Ga_{0.4}B_{5.6}$ nanocomposites, the annealing at 715^{o}C for 4 min leads to a slight increase, both in remanent magnetisation and in coercivity, but the increased value of 0.62 for M_r/M_S ratio proves that a greater fraction of soft and hard magnetic phases is exchanged coupled.

Summary

Magnetic microstructure of melt-spun (Nd,Pr,Dy)-(Fe,Co,Ga)-B ribbons is very sensitive to variable Nd and Fe contents in comparison with previously published Mössbauer spectroscopic studies of $Nd_2Fe_{14}B$, where average internal magnetic field $<B_{hf}>_{at}$ 295K is estimated as 30.4 T [18,19]. There is a close agreement of $<B_{hf}>_{at}$ 294 K, estimated as 29.4 T and 28.0 T for $Nd_2Fe_{14}B$, dominantly present in $Nd_{13.7}Pr_{0.7}Dy_{0.2}Fe_{73.1}Co_{6.3}Ga_{0.4}B_{5.6}$ and $Nd_{7.7}Pr_{0.7}Dy_{0.2}Fe_{79.1}Co_{6.3}Ga_{0.4}B_{5.6}$ nanocomposites, respectively. It is worthy to note that the volume fraction of Fe_3B remains almost same and the formation of mostly formed tetragonal Fe_3B contributes to the enhancement of total magnetization of the nanocomposite magnets [20]. The $Nd_{1.1}Fe_4B_4$ doublets are with an evident change of quadruple splitting 1.24(5) mm/s and 1.37(4) mm/s, FWHM of about 0.26(3) mm/s ($Nd_{13.7}Pr_{0.7}Dy_{0.2}Fe_{73.1}Co_{6.3}Ga_{0.4}B_{5.6}$) and 0.32(6) mm/s ($Nd_{7.7}Pr_{0.7}Dy_{0.2}Fe_{79.1}Co_{6.3}Ga_{0.4}B_{5.6}$) and an almost constant relative concentration for both nanocomposites, respectively. So, they correspond to a distinct phase which becomes

paramagnetic at room temperature. The α-Fe fraction decrease from 13.1(9)% in $Nd_{13.7}Pr_{0.7}Dy_{0.2}Fe_{73.1}Co_{6.3}Ga_{0.4}B_{5.6}$ to 6.5(1)% in $Nd_{7.7}Pr_{0.7}Dy_{0.2}Fe_{79.1}Co_{6.3}Ga_{0.4}B_5$ has influence on the sharp decrease of the magnetic performances: reduced remanence and intrinsic coercitivity [21,22]. The substitution of Fe by Co in the hard magnetic phase is highlighted by the values of the Curie temperatures determined for the $Nd_{13.7}Pr_{0.7}Dy_{0.2}Fe_{73.1}Co_{6.3}Ga_{0.4}B_{5.6}$ and $Nd_{7.7}Pr_{0.7}Dy_{0.2}Fe_{79.1}Co_{6.3}Ga_{0.4}B_5$ samples: 365^{o}C respectively 355^{o}C, greater than 312^{o}C, the Curie temperature of the $Nd_2Fe_{14}B$ compound. The crystallisation temperatures of the soft magnetic phases existing in the nanocomposites are situated at 564.5^{o}C, respectively 568^{o}C $Nd_{13.7}Pr_{0.7}Dy_{0.2}Fe_{73.1}Co_{6.3}Ga_{0.4}B_{5.6}$ and $Nd_{7.7}Pr_{0.7}Dy_{0.2}Fe_{79.1}Co_{6.3}Ga_{0.4}B_{5.6}$ melt spun samples. The magnetic properties, measured at room temperature on the quenched and annealed ribbons, revealed the relationship between the alloy chemical composition and processing. The parameters of the recrystallization process could be carefully chosen in the case of the studied nanocomposites, in order to lead to an improvement of the magnetic performances of the as-quenched NdFeB-based alloys. Analysis of experimental results enabled better insight in relationship between microstructure and magnetic properties of nanocomposites, function of variable percentage fraction of iron.

Acknowledgement
This work has been supported by grant No. 171001G from Serbian Ministry of Science and Technological Development, by Romanian grant 14N 5201/2016 and Romania–JINR Dubna project No. 47/2015, from Romanian Ministry of Research-Development and Innovation.

References

[1] K. J. Strnat, G. Hoffer, J. Oson, W. Ostertag, A family of new cobalt-base permanent magnet materials, J. Appl. Phys. 38 (1967) 1001-1002. https://doi.org/10.1063/1.1709459

[2] M. Sagawa, S. Fujimura, N. Togawa, H. Yamamoto, Y. Matsuura, New material for permanent magnets on a base of Nd and Fe, J. Appl. Phys. 55 (1984) 2083-2087. https://doi.org/10.1063/1.333572

[3] J.J. Croat, J.F. Herbst, R.W. Lee, F.E. Pinkerton, Pr-Fe and Nd-Fe-based materials: A new class of high-performance permanent magnets, J. Appl. Phys. 55 (1984) 2078–2080. https://doi.org/10.1063/1.333571

[4] F.E. Pinkerton, W.R. Dunham, Mössbauer effect in $R_2Fe_{14}B$ compounds, J. Appl. Phys. 57 (1985) 4121-4123. https://doi.org/10.1063/1.334638

[5] W. Kappel, M.M. Codescu, D. Popa, Losses in sintered NdFeB magnets, Rom. Rep. Phys. 56 (2004) 391–398.

[6] W. Kappel, M.M.Codescu, N. Stancu, D. Popa, Evaluation of the corrosion behavior of the permanent magnets based on rare earths, used in aeronautical industry, J. Optoelectron. Adv. Mat. 8 (2006) 523–526.

[7] M.M. Codescu, W. Kappel, D. Popa, Corrosion tests on alloys and permanent magnets based on NdFeB, used in aerospace industry, J. Optoelectron. Adv. Mat. 10 (2008) 790-793.

[8] H.A. Davies, A. Manaf, P.Z. Zhang, Nanocrystallinity and magnetic property enhancement in melt-spun iron-rare earth-base hard magnetic alloys, J. Mater. Eng. Perform. 2 (1993) 579-587. https://doi.org/10.1007/BF02661744

[9] G.C. Hadjipanayis, Nanophase hard magnets, J. Magn. Magn. Mater. 200 (1999) 373-391. https://doi.org/10.1016/S0304-8853(99)00430-8

[10] J.F. Herbst, $R_2Fe_{14}B$ materials: Intrinsic properties and technological aspects, Rev. Mod. Phys. 63 (1991) 819-898. https://doi.org/10.1103/RevModPhys.63.819

[11] I.R. Betancourt, H.A. Davies, Magnetic properties of nanocrystalline didymium (Nd-Pr)-Fe-B alloys, J. Appl. Phys. 85 (1999) 5911-5913. https://doi.org/10.1063/1.369911

[12] Z.C. Wang, M.C. Zhang, F.B. Li, S.Z. Zhou, R. Wang, W. Gong, High-coercivity $(NdDy)_2(FeNb)_{14}B$–α–Fe nanocrystalline alloys, J. Appl. Phys. 81 (1997) 5097-5099. https://doi.org/10.1063/1.365187

[13] J.M. Yao, T.S. Chin, Coercivity of Ti-modified (α-Fe)-$Nd_2Fe_{14}B$ nanocrystalline alloys, J. Appl. Phys. 76 (1994) 7071-7073. https://doi.org/10.1063/1.358030

[14] A. Inoue, A. Kojima, A. Takeuchi, T. Masumoto, A. Makino, Hard and soft magnetic properties of nanocrystalline Fe–Nd–Zr–B alloys containing intergranular amorphous phase, J. Appl. Phys. 79 (1996) 4836-4836. https://doi.org/10.1063/1.361624

[15] I. Panagiatopoulos, L. Withanawasam, A. S. Murthy, G.S. Hadjipanayis, E.W. Singleton, D.J. Sellmyer, Magnetic hardening of melt-spun nanocomposite Nd2Fe14B/Fe magnets, J. Appl. Phys. 79 (1996) 4827-4829. https://doi.org/10.1063/1.361621

[16] T. Schrefl, J. Fidler, Födermayr, Modelling of exchange-spring permanent magnets, J. Magn. Magn. Mater. 177-181 (1998) 970-975. https://doi.org/10.1016/S0304-8853(97)00653-7

[17] R.A. Brand, (2008) WinNormos Mössbauer fitting program, Universität Duisburg.

[18] C. You, X.K. Sun, W. Liu, B. Cui, X. Zhao, D. Geng, Z. Zhang, Effects of W and Co additions on the phase transformation and magnetic properties of nanocomposite $Nd_2Fe_{14}B$/α-Fe magnets, J. Phys. D: Appl. Phys. 35 (2002) 943-950. https://doi.org/10.1088/0022-3727/35/10/301

[19] B. Cekič, V. Ivanovski, M.M. Codescu, A. Umicevic, T. Barudzija, E.A. Patroi, Mössbauer Spectroscopic Analysis of $Nd_2Fe_{14}B$/α-Fe Hard Magnetic Nanocomposites, Sol. St. Phen. 170 (2011) 154-159. https://doi.org/10.4028/www.scientific.net/SSP.170.154

[20] R. Kamal, Y. Andersson, Mössbauer spectroscopic studies of $Nd_2Fe_{14}B$, Phys. Rev. B 32 (1985) 1756-1760. https://doi.org/10.1103/PhysRevB.32.1756

[21] W. Kappel, M.M. Codescu, $Nd_2Fe_{14}B$/α-Fe Hard Magnetic Nanocomposite. Performances and Limits, Rom. J. Phys. 49 (2004) 733-741.

[22] W. Kappel, M.M. Codescu, M. Valeanu, N. Stancu, J. Pintea, F. Lifei, A. Jianu, D. Patroi, E. Patroi, Influence of the recrystallization processes on the structure and magnetic properties of the $Nd_2Fe_{14}B$/alpha-Fe nanocomposites, J. Optoelectron. Adv. Mat. 9 (2007) 1825-1828.